JOURNAL OF SOLID STATE CHEMISTRY **125,** 67–74 (1996)
ARTICLE NO. 0266

Cationic Distribution and Oxidation Mechanism of Trivalent Manganese Ions in Submicrometer $Mn_xCoFe_{2-x}O_4$ Spinel Ferrites

M. Laarj and S. Kacim

Département de Chimie, Faculté des Sciences Semlalia, B.P. S15, Marrakech, Morocco

and

B. Gillot

Laboratoire de Recherche sur la réactivité des Solides, URA 23 Faculté des Sciences Mirandes, B.P. 138, 21004 Dijon Cedex, France

Received January 3, 1996; in revised form March 18, 1996; accepted May 14, 1996

Submicrometer $Mn_xCoFe_{2-x}O_4$ ($0 \leq x < 1$) spinel particles with a spherical shape were prepared at low temperature from oxalic precursors. Because of their small crystallite size (about 50 nm), these ferrite particles can be oxidized below 400°C giving cubic deficient spinels having both Mn^{3+} and Mn^{4+} ions because of oxido-reduction phenomena. Information about the valence state of the manganese and cobalt ions and cation distribution between tetrahedral (*A*) and octahedral (*B*) sites are derived from lattice parameter variation, IR spectroscopy, thermogravimetric analysis, and electrical conductivity. A kinetics study of the oxidation of Mn^{3+} ions shows that oxidation proceeds by cation diffusion through a topotactic reaction with a constant chemical diffusion coefficient for $x < 0.60$ and variable above $x = 0.80$ and an activation energy close to 115 kJ mol^{-1} but, however, depending on manganese substitution content.

1. INTRODUCTION

Recently, the thermal behavior of submicrometer $Mn_xCo_yFe_{3-x-y}O_4$ ($0 \leq x < 1$, $0 \leq y < 1$) and $Mo_xCo_y Fe_{3-x-y}O_4$ ($0 \leq x < 0.63$, $0 < y \leq 0.90$) ferrites with spinel structure during their oxidation in cation deficient spinels has been studied (1–3). The originality of these compounds, in comparison with other defect ferrites, is that the vacancies result not only from the oxidation of iron ions but also from the oxidation of manganese or molybdenum ions. These vacancies enhance or hinder, depending on the cooling down rate, the movement of cobalt ions between equivalent cations sites and largely determine the original properties of these non-stoichiometric spinels, such as their magnetic and electrical properties (4–7).

In contrast to the case of $CoFe_2O_4$, where Co^{2+} and Fe^{3+} ions have great stability toward oxidation, for submicrometer manganese ferrites with or without cobalt, Fe^{2+}, Mn^{2+}, and Mn^{3+} ions can be oxidized between 200 and 450°C into Fe^{3+}, Mn^{3+}, and Mn^{4+} ions, respectively, giving defect spinel ferrites (8, 9). However, beyond 450°C, Mn^{4+} ions are not stable and are reduced to Mn^{3+} ions (8, 10). In the same manner, manganese ions can be oxidized or reduced in finely ground manganese cobaltites or cobalt manganites (11, 12) and cation vacancies appear in the spinel structure when Mn^{n+} ions oxidize into $Mn^{(n+1)+}$ ions ($n = 2$ or 3).

In this paper, we report investigations on the series $Mn_xCoFe_{2-x}O_4$. The substitution of iron by manganese in $CoFe_2O_4$ is expected to give rise to an increase in the Mn^{3+} concentration leading to the compounds $Mn_xCoFe_{2-x}O_4$ ($0 \leq x \leq 1$) for which, in contrast to the case of pure submicrometer $Mn_xFe_{3-x}O_4$ ($0 \leq x \leq 1$) ferrites, there was no other oxidation partly superimposed on the oxidation of Mn^{3+} ions. It is then possible to study the oxidation kinetics of Mn^{3+} ions with maintenance of the spinel structure when all other cations maintain their initial oxidation state.

2. EXPERIMENTAL DETAILS

Ferrite particles with spherical shapes were prepared via decomposition of mixed oxalate precursors $Co_{1/3}Mn_{x/3}Fe_{(2-x)/3}C_2O_4, 2H_2O$ ($0 \leq x < 1$) in air flow up to 650°C. After this treatment the powders were reduced at around 300°C in a mixture of nitrogen, hydrogen, and steam in proportions (80 : 8 : 12). The reduction temperature was slightly modified according to the manganese content in order to reach the stoichiometry without formation of CoO extra phase, revealed for the "too reduced" samples. The phase formation was checked by X-ray diffraction using CuKα radiation. The composition of the samples

0022-4596/96 $18.00

TABLE 1
Cobalt and Manganese Content Data, Composition x, Lattice Parameter (a), and Crystallite Size of the Spinels Investigated

Sample code	Cobalt (mass%)	Manganese (mass%)	$Mn_xCoFe_{2-x}O_4$	X	Lattice parameter (a) in nm	Crystallite size in nm
M0	25.10	0	$CoFe_2O_4$	0	0.8398	49
M7	25.33	6.67	$CoMn_{0.26}Fe_{1.74}O_4$	0.26	0.8410	50
M9	25.64	8.92	$Co_{0.99}Mn_{0.36}Fe_{1.65}O_4$	0.36	0.8412	47
M12	26	11.59	$Co_{1.03}Mn_{0.48}Fe_{1.49}O_4$	0.48	0.8419	50
M15	25.33	15.30	$Co_{0.98}Mn_{0.64}Fe_{1.38}O_4$	0.64	0.8424	51
M21	24.86	21.30	$Co_{1.02}Mn_{0.90}Fe_{1.08}O_4$	0.90	0.8433	52

(Table 1) were analyzed by atomic absorption spectroscopy after dissolving the ferrite powders in a concentrated HCl solution. The average particle size of these loose powders was measured from enlarged scanning microscopy (SEM) images as 50 nm (Table 1).

The oxidations were performed in a Setaram MTB 10-8 microbalance with 20 mg powder using a heating rate of 2°C min^{-1} or under isothermal conditions. The oxidation degree of the samples at various levels of reaction was calculated from the gravimetric data. Fourier transform infrared (FTIR) spectra were recorded with a Perkin–Elmer 1725X spectrometer and the Csl disk technique. The dc conductivity measurements were carried out under vacuum or O_2 atmosphere on compressed disks using a two-probe technique described elsewhere (13).

3. RESULTS AND DISCUSSION

3.1. Cationic Distribution

Samples with cubic spinel structure were obtained in the compositional range $0 < x < 1$. The lattice parameter (a) values are summarized in Table 1 and its dependence as a function of the manganese content x is depicted in Fig. 1 (curve a). Vegard's law is approximately obeyed. Figure 1 (curve b) shows also the experimental $a = f(x)$ curves for submicrometer $Mn_xCoFe_{2-x}O_4$ spinel particles with an acicular shape (2).

Infrared studies indicate the presence of two pronounced absorption bands υ_1 and υ_2 in the range 700–300 cm^{-1} which are found in the expected range as shown in Fig. 2 for a spinel-type ternary oxide with space group $Fd3m$-O_h^7 (14). It has been reported previously that for inverse II–III spinels such as $CoFe_2O_4$ the high-frequency band υ_1 belongs to the tetrahedral sites and the low-frequency band υ_2 to the octahedral complexes (15, 16). It appears that the introduction of manganese into the cobalt ferrite lattice in place of iron has only a small effect on the position of these bands υ_1 and υ_2. This indicates that the cation distribution and their valencies were not deeply modified by manganese substitution.

It is seen from Fig. 2 that besides the main high-frequency band υ_1 there are two sidebands υ_1' and υ_2'. The existence of the sidebands can be considered as evidence of Co^{2+} ions being present in tetrahedral sites as well, leading to the splitting of the υ_1 band which is known to be connected to threefold degenerate intrinsic vibrations of tetrahedral complexes (17).

This leads to the conclusion that the cation distribution for $Mn_nCoFe_{2-x}O_4$ to a first approximation can be formulated as

$$(Co_y^{2+}\, Fe_{1-y}^{3+})_A\, (Fe_{1-x+y}^{3+}\, Mn_{1-y}^{3+}\, Co_{2-y}^{3+})_B\, O_4^{2-}. \qquad [1]$$

To prove more strictly the assumption of Co^{2+} ions in

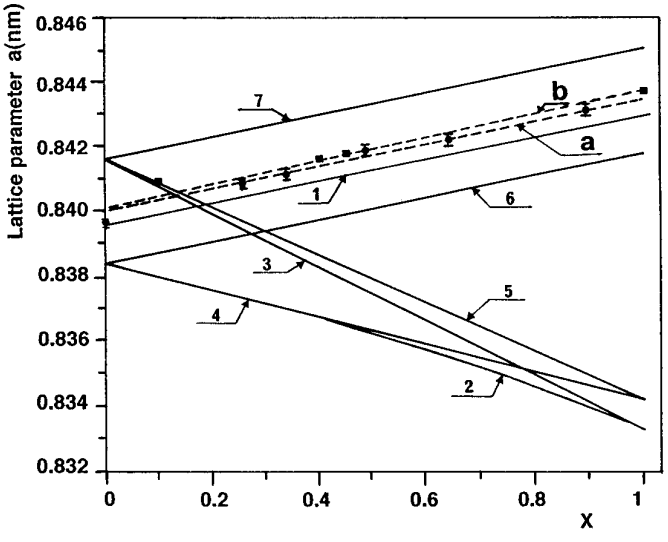

FIG. 1. Lattice parameter (a) of $Mn_xCoFe_{2-x}O_4$ spinels versus manganese content. Experimental points (●), spherical particles (this work); (■) acicular particles, Ref. (2) and calculated curves assuming the following structural formulas [1] with $y = 0.3$ and [2]–[7].

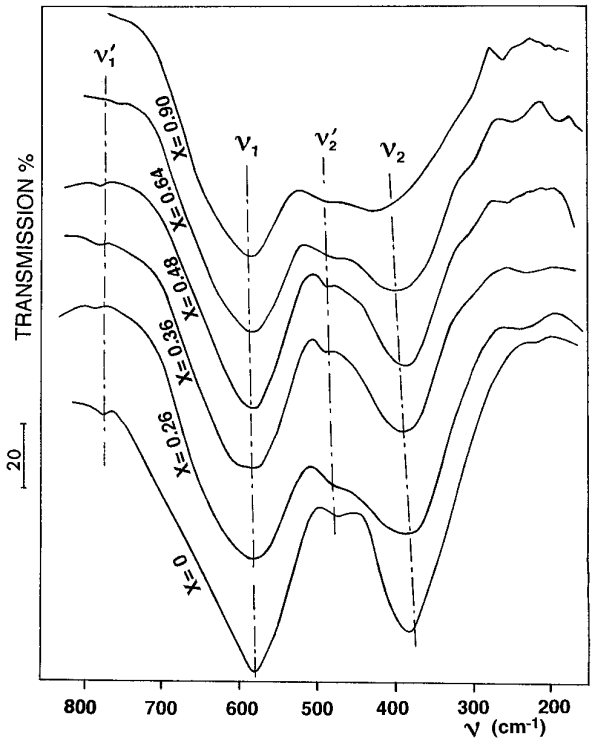

FIG. 2. FT-IR spectra of the $Mn_xCoFe_{2-x}O_4$ system.

A sites, the theoretical lattice parameters (a) as function of manganese content are calculated for different structural formulas. After Kulkarni (18), the manganese and cobalt ions in $CoMnFeO_4$ ($x = 1$) have the III and II valences, respectively. However, the substitution of iron by manganese in $CoFe_2O_4$ can be done, *a priori,* according to two different mechanisms. In the first, Fe^{3+} ions are replaced by Mn^{3+} ions, and in the second, the (Co^{2+}, Fe^{3+}) pairs are replaced by (Co^{3+}, Mn^{2+}). Indeed the II and III valence states of manganese may be expected in stoichiometric ferrites (8, 9). Only octahedral Co^{3+} ions were taken into account, because of their B-site preference (19, 20). On the other hand, the fourfold and sixfold Mn^{2+} and Co^{2+} ions were considered. Consequently, considering the cation locations in both sublattices, the six structural formulas.

$$(Mn_x^{2+}\, Fe_{1-x}^{3+})_A\, (Fe^{3+}\, Co_{1-x}^{2+}\, Co_x^{3+})_B\, O_4^{2-} \quad [2]$$

$$(Mn_x^{2+}\, Co_{1-x}^{2+})_A\, (Fe_{2-x}^{3+}\, Co_x^{3+})_B\, O_4^{2-} \quad [3]$$

$$(Fe^{3+})_A\, (Fe_{1-x}^{3+}\, Mn_x^{2+}\, Co_{1-x}^{2+}\, Co_x^{3+})_B\, O_4^{2-} \quad [4]$$

$$(Fe_x^{3+}\, Co_{1-x}^{2+})_A\, (Fe_{2-2x}^{3+}\, Mn_x^{2+}\, Co_x^{3+})_B\, O_4^{2-} \quad [5]$$

$$(Fe^{3+})_A\, (Fe_{1-x}^{3+}\, Mn_x^{3+}\, Co_x^{2+})_B\, O_4^{2-} \quad [6]$$

$$(Co^{2+})_A\, (Fe_{2-x}^{3+}\, Mn_x^{3+})_B\, O_4^{2-} \quad [7]$$

may be considered.

Lattice parameters were calculated by using the invariant character of the "cation–anion" distances established by Poix (21, 22) from a systematic study of spinel structures (Table 2). Two parameters are thus defined giving the average value of the cation–oxygen distances for A and B sites

$$d_A = a\sqrt{3}\left(\frac{1}{8} + \delta\right) \quad [8]$$

$$d_B = a\left(\frac{1}{16} - \delta/2 + 3\delta^2\right)^{1/2}, \quad [9]$$

where a is the lattice parameter and $\delta = u - 3/8$ with u the oxygen position. d_A and d_B can be also expressed explicitly as a function of the cation distributions and the cation–anion distance

$$d_A = \Sigma\, C_i^A (Me_i - O)_4 \quad \text{for tetrahedral sites} \quad [10]$$

$$2d_B = \Sigma\, C_i^B (Me_i - O)_6 \quad \text{for octahedral sites,} \quad [11]$$

C_i^A and C_i^B being the concentrations of the metallic cations Me, respectively, at A and B sites ($\Sigma\, C_i^A = 1$, $\Sigma\, C_i^B = 2$). By solving the system of Eqs. [10] and [11], Poix has established the following equation:

$$a = 2.0995\, d_A + (5.8182\, d_B^2 - 1.4107\, d_A^2)^{1/2}. \quad [12]$$

As shown in Fig. 1, the calculated curves for the [2] to [5] distributions have a slope opposite to that of the experimental curve showing that the formulas tested are unable to describe the cation distribution. Assuming the substitution of Fe^{3+} ions by Mn^{3+} ions in B sites according to octahedral preference of Mn^{3+} ions (23), this agreement is better for formulas [6] and [7] (Fig. 1). However, the experimental points are situated between these two theoretical curves. Therefore, for these spinels, the Co^{2+} ions seem to be located at both B and A sites as predicted by

TABLE 2
Cation–Oxygen Distances Used to Calculate the Theoretical Value of the Lattice Parameter

Anion–cation bonds	B site (nm)	A site (nm)
Mn^{2+}–O	0.2220	0.2041
Mn^{3+}–O	0.2045	
Mn^{4+}–O	0.1843	
Co^{2+}–O	0.2123	0.1974
Co^{3+}–O	0.1892	
Fe^{3+}–O	0.2020	0.1858
□–O	0.2240	

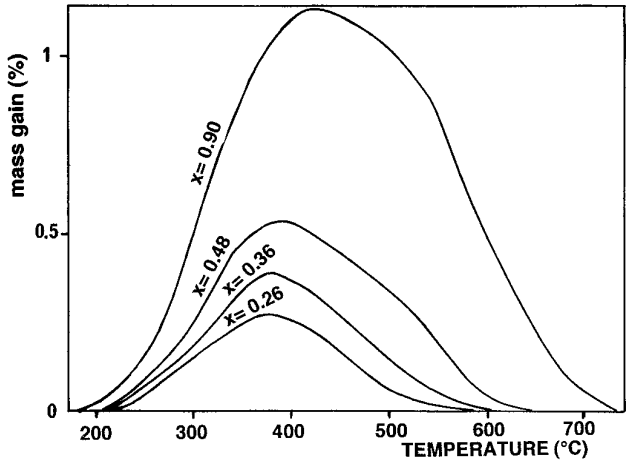

FIG. 3. Dependence of the mass gain on temperature for $Mn_xCoFe_{2-x}O_4$ spinels.

IR spectroscopy. A recent study by neutron diffraction has confirmed for the composition $x = 0.36$ (24), the presence of a not negligible (0.30) fraction y of Co^{2+} ions located at A sites. If we assume an identical fraction for all x values, we can calculated from Poix's method the theoretical lattice parameter (Fig. 1, curve 1). The better agreement found between curve 1 and curve a outlines the reliability of the cation distribution given in formula [1].

3.2. Oxidative Nonstoichiometry of Mn^{3+} Ions

3.2.1. Thermogravimetric study. Thermogravimetric analysis in nonisothermal oxidation conditions performed in a static atmosphere of pure O_2 shows a mass gain from 200 to 400°C increasing with the manganese content (Fig. 3) and the oxygen pressure (Fig. 4). Because no oxidation was observed for pure $CoFe_2O_4$, this mass gain is ascribed to the oxidation of Mn^{3+} ions into Mn^{4+} ions. A study by differential thermogravimetry (DTG) shows that this reaction (Fig. 5, curve a) occurs in the same range of temperature as for the oxidation of octahedral Mn^{3+} ions in Mn ferrites (Fig. 5, curve b) having the same particle shapes and crystallite sizes. Indeed, a close examination of the influence of cobalt substitution reveals that not only the top of the Mn^{3+} ions oxidation peak is located at an identical temperature (340°C) but also that the substitution removed the oxidation peaks of Fe^{2+} and Mn^{2+} ions. In this study the two considered cation distributions can be formulated as (8)

$$(Co^{3+}_{0.3}\, Fe^{3+}_{0.7})_A\, (Mn^{3+}_{0.9}\, Co^{2+}_{0.7}\, Fe^{3+}_{0.4})_B\, O^{2-}_4 \qquad [13]$$

and

$$(Mn^{2+}_{0.8}\, Fe^{3+}_{0.2})_A\, (Mn^{3+}_{0.2}\, Fe^{2+}_{0.2}\, Fe^{3+}_{1.6})_B\, O^{2-}_4. \qquad [14]$$

It is apparent that because the Co substitution replaced the divalent Fe^{2+} and Mn^{2+} ions, solely the Mn^{3+} ions oxidation peak was detected in the DTG curves. Moreover, the presence of Mn^{4+} ions is confirmed by the reduction peak (Fig. 5, curve a) and the mass loss (Figs. 3 and 4) observed beyond 400°C. For Mn ferrites it has been established that Mn^{2+} ions oxidized in two steps (8) (Fig. 5, curve b), the second step taking place at about 650°C with a phase transformation.

The Mn^{3+} ion oxidation is only partial as shown in Fig.

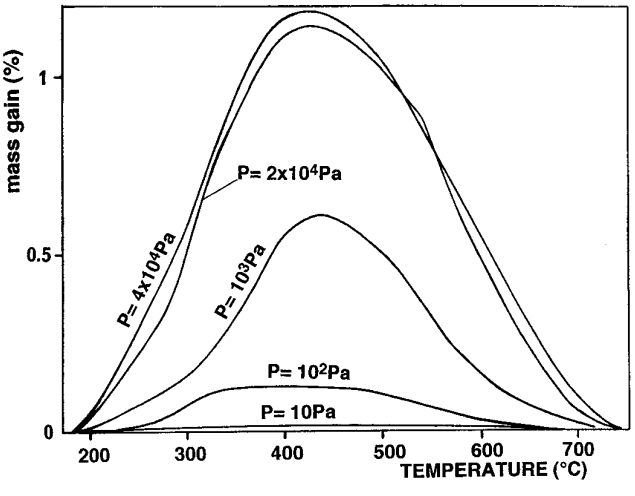

FIG. 4. Dependence of the mass gain on temperature for $Mn_{0.9}CoFe_{1.1}O_4$ spinel as function of oxygen pressure.

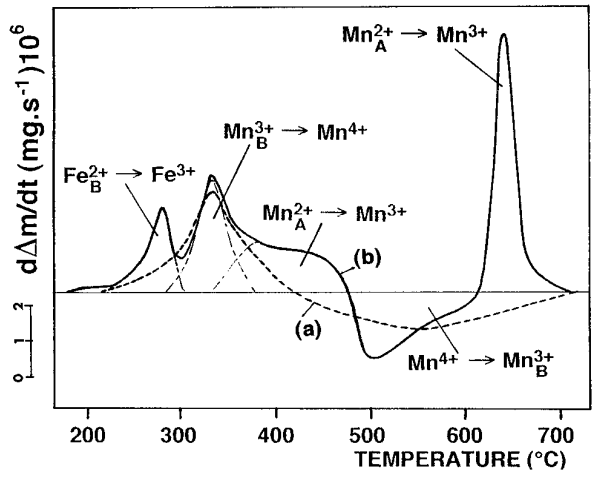

FIG. 5. DTG curves of samples heated in pure O_2($PO_2 = 2 \times 10^4$ Pa) at a linear rate of 2°C min^{-1}. (——) $MnFe_2O_4$ spinel, (------) $Mn_{0.9}CoFe_{1.1}O_4$ spinel.

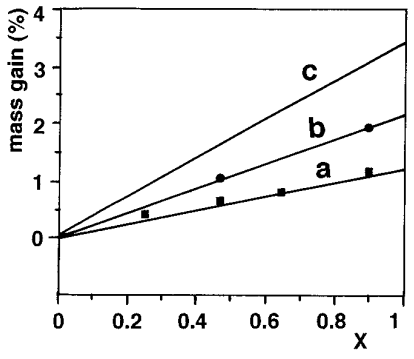

FIG. 6. Comparison of measured under (a) nonisothermal and (b) isothermal conditions with calculated (c) mass gain, assuming total oxidation of Mn^{3+} ions into Mn^{4+} ions.

6 (curve a). Consequently the ferrites oxidized around 350°C have both Mn^{3+} and Mn^{4+} ions in their lattice. The resulting formula deduced from Eq. [1] with $y = 0.3$ can be expressed as

$$(Co^{2+}_{8y/D}\ Fe^{3+}_{(8(1-y)+\delta x)/D})_A$$
$$(Fe^{3+}_{(8(1-x+y)-\delta x)/D}\ Mn^{3+}_{(8x(1-\delta))/D}\ Mn^{4+}_{8\delta x/D}\ Co^{2+}_{8(1-y)/D}\ \square_{3\delta x/D})_B\ O^{2-}_4. \quad [15]$$

δ is the fraction of oxidized manganese ions, (δ = number of Mn^{4+} ions/total number of Mn^{3+} and Mn^{4+} ions), $D = 8 + \delta x$, and $\square$ is the cationic vacancy.

3.2.2. Electrical behavior. Figure 7 compares the evolution with temperature of the electrical conductivity (σ) under vacuum and under oxygen (curves a). Under vacuum, the logarithm of the electrical conductivity shows a linear relationship with T^{-1} (curve 1a) between 200 and 500°C, according to the semiconductor behavior $\sigma = \sigma_0 \exp(-E_\sigma/kT)$ in which E_σ is the activation energy of conduction. In contrast, in the presence of oxygen, starting with unoxidized spinel at low temperature, this relation was not obeyed beyond 290°C (curve 2a) consequent to the oxidation of Mn^{3+} ions. Above this temperature, Mn^{4+} ions are also present that induce an increase in the number of Mn^{3+}–Mn^{4+} pairs and the conductivity, which proceeds via hopping of charge carriers, increases more rapidly. At about 380°C the conductivity is maximum. Then at higher temperature, the number of Mn^{3+}–Mn^{4+} pairs decreases, leading to a correlative decrease in the conductivity. This particular evolution where the conductivity will reach a maximum when the number of Mn^{3+} ions is equal to the number of Mn^{4+} ions (25) is confirmed in isothermal oxidation at 350°C (Fig. 7, curve b). In this case a rapid increase of the conductivity is also noted which can be correlated with the oxidation of Mn^{3+} ions at B sites. After partial oxidation of Mn^{3+} ions, we observe a decrease of conductivity due to a diminishing of Mn^{3+}–Mn^{4+} pairs resulting from the reduction process.

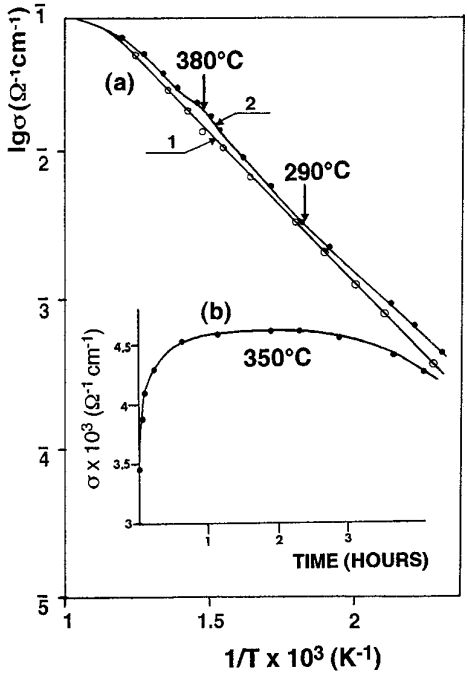

FIG. 7. (a) Temperature dependence of the dc electrical conductivity for a $Mn_{0.9}CoFe_{1.1}O_4$ spinel, (1) under vacuum and (2) under O_2 atmosphere; (b) Kinetics curve $\sigma = f(t)$ for oxidation of octahedral Mn^{3+} ions.

3.2.3. Infrared investigation. Figure 8 depicts the profile of the IR spectra of samples with $x = 0.90$ oxidized at

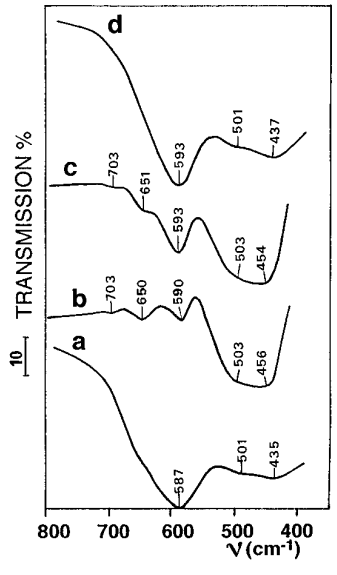

FIG. 8. FT-IR spectra of oxidized $Mn_{0.9}CoFe_{1.1}O_4$ spinel in the 800–400 cm^{-1} region (a) at 300°C for 4 h, (b) at 300°C for 24 h, (c) at 300°C for 48 h, and (d) at 780°C for 8 h.

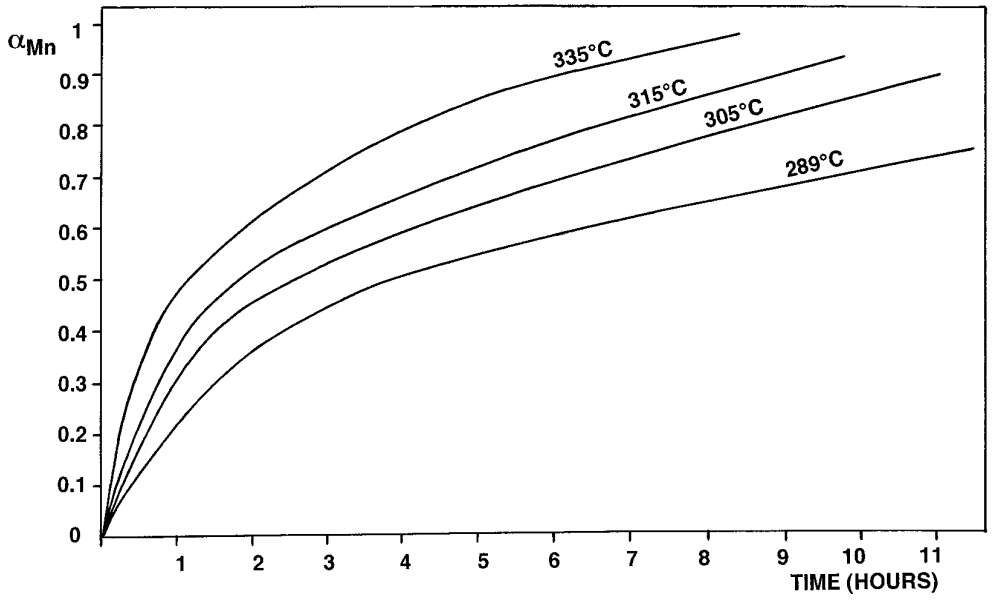

FIG. 9. Kinetics curves $\alpha_{Mn} = f(t)$ for octahedral Mn^{3+} ion oxidation for spinel $Mn_{0.48}CoFe_{1.52}O_4$.

330°C (curves a, b, c) for various heating times. For a reaction time of 4 h (curve a) leading to a degree of oxidation at about 20% (Mn^{4+}/Mn^{3+} ratio), the spectrum exhibits two intense bands at 587 and 435 cm^{-1} and one band of lower intensity at 501 cm^{-1}. This behavior is similar to the spectrum of unoxidized sample (Fig. 2). With increasing degree of oxidation (but not exceeding 50%), two absorption bands at 650 and 703 cm^{-1} are observed (curves b and c). The appearance of these additional bands apparently results from the presence of Mn^{4+} ions. High-frequency bands associated with the presence of tetravalent cations on octahedral sites also are observed for synthetic γ-MnO_2 (26) and molybdenum substituted magnetites (27). However, for reaction times beyond 24 h, there is evidence that the intensity of these two bands decrease (curve c) whereas the intensity of the band at 593 cm^{-1} attributed to the unoxidized spinel increases. This behavior may be correlated to a beginning of reduction of Mn^{4+} ions. With in-

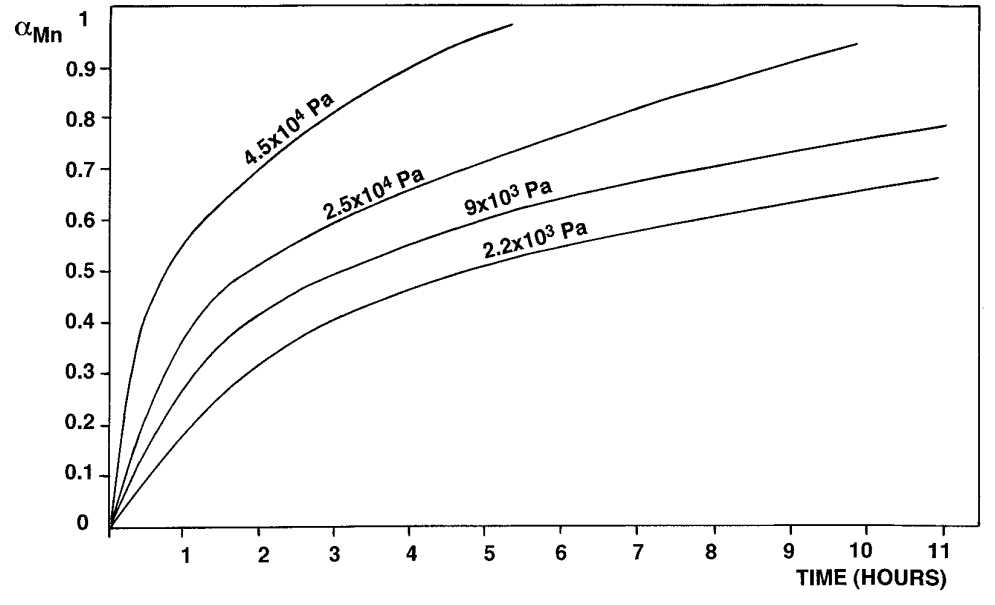

FIG. 10. $\alpha_{Mn} = f(t)$ curves for spinel $Mn_{0.48}CoFe_{1.52}O_4$: pressure law.

creasing treatment temperature (curve d) a complete disappearance of the two high frequency bands occurs while the IR spectrum of the unoxidized sample again is well apparent. This indicates that after this stage, stoichiometric Mn–Co ferrite is obtained.

3.3. Isothermal Kinetics Analysis

Higher values of δ can be reached when isothermal oxidations are carried out around 350°C (Fig. 6, curve b). However it was not possible to oxidize the Mn^{3+} ions completely and the higher value of δ was 0.57 for $x = 0.90$ after an oxidation at 360°C for 40 h.

The oxidation kinetics curves $\alpha_{Mn} = f(t)$ determined as function of temperature and oxygen pressure have a roughly parabolic shape (Figs. 9 and 10). The conversion rate is defined as $\alpha_{Mn} = W_t/W_\infty$ where W_t is the amount of Mn^{3+} ions oxidized to Mn^{4+} ions in time t, and W_∞ is the corresponding amount after 40 h of reaction. Such an oxidation can be analyzed as a vacancy diffusion-controlled process obeying the usual Fick's equations with a concentration given at the surface by thermodynamic conditions (7). It has been shown that when the chemical diffusion coefficient, $\tilde{D}$, is constant the kinetics curves for spherical particles can be described by the expression (28)

$$\alpha_{Mn} = 1 - 6/\pi^2 \sum_{n=1}^{\infty} (1/n^2) \exp(-n^2 kt), \qquad (16)$$

where $k = \pi^2\tilde{D}/r^2$ and r is the mean grain radius.

The experimental curves can be directly compared to the theoretical curves $\alpha_{Mn} = f(t/t_{1/2})$, where $t_{1/2}$ is the half reaction time. Figure 11 shows for $x = 0.48$ (curves 1) the comparison between the experimental curves and those obtained by fitting. This figure reveals clearly that the two sets of curves are in reasonable agreement. However, for $x = 0.90$, the two sets of curves agree less (curves 2). Compared in the case of a constant chemical diffusion coefficient, the diffusion is faster at the beginning of the reaction (curve 2a) before slowing down at the end (curve 2b). For this composition, it is not possible to model the oxidations by considering a constant chemical diffusion coefficient. Such oxidation behavior, already observed for ferrites containing molybdenum or vanadium (29), has been explained on the basis of very significant stresses generated in the particles by the chemical gradient induced during the oxidation mechanism (30). These stresses are due to the difference in the degree of oxidation between the beginning and the end of the reaction (the surface being more oxidized than the bulk) leading to a diffusion coefficient smaller in the bulk of the material than at the surface. In this respect, we consider that, consequently to the formation of a higher concentration in vacancies per molecule for the composition $x = 0.90$ as calculated from

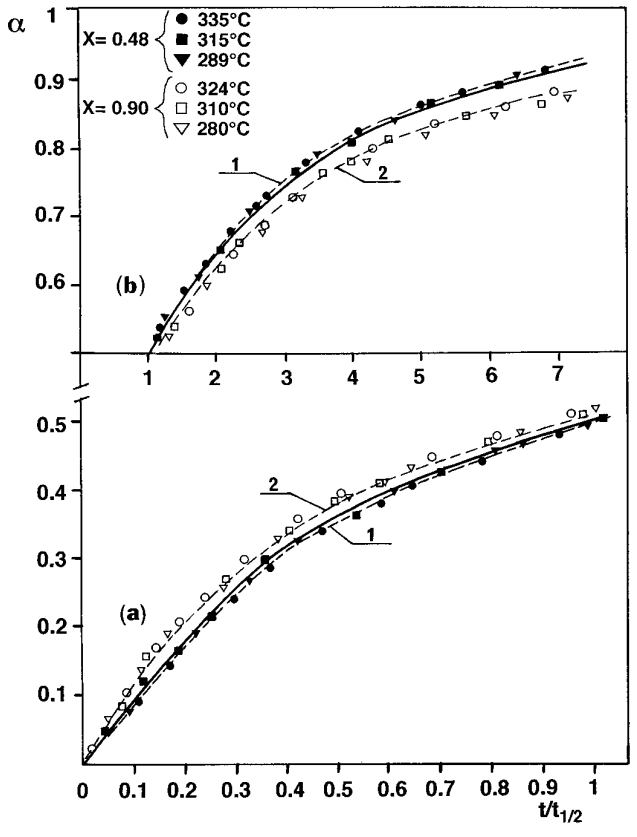

FIG. 11. Theoretical curves $\alpha = f(t/t_{1/2})$ for the case of a three-dimensional isotropic diffusion with $\tilde{D}$ constant (Eq. [16]) and experimental data for $Mn_xCoFe_{2-x}O_4$ spinels with (1): $x = 0.48$ and (2) $x = 0.90$.

Eq. [15] (0.18 for $x = 0.90$ and 0.085 for $x = 0.48$), the lattice parameter more sharply decreases as observed experimentally ($\Delta a = 0.034$ nm for $x = 0.90$ and 0.026 nm for $x = 0.48$ (2).

From the variation of ln $\tilde{D}$ versus $1/T$ an activation energy of 110 kJ mol^{-1} was obtained for $x = 0.48$ and 122 kJ mol^{-1} for $x = 0.90$. These values are slightly higher than the activation energy of Fe^{2+} ions oxidation in magnetite particles (31) having the same crystallite size as in the $Mn_xCoFe_{2-x}O_4$ ferrites studied.

4. CONCLUSION

The valuence states of the manganese and cobalt ions in submicrometer $Mn_xCoFe_{2-x}O_4$ spinel ferrites are +III and +II, respectively. The Mn^{3+} ions are located in octahedral sites while the Co^{2+} ions may be located in both octahedral and tetrahedral sites. These results are consistent with the interpretation given by Martens (32), for the magneto-optical properties at 800 nm of $CoMn_xFe_{3-x}O_4$ ferrites on one hand, and with the oxidation behavior of the studied samples on the other hand. Indeed, the manganese ions

are oxidized in the spinel lattice, at the same temperature as the Mn^{3+} ions in the $Mn_xFe_{3-x}O_4$ ferrites having the same crystallite sizes. Moreover, beyond 400°C the resulting defect ferrites are reduced, confirming the formation of unstable Mn^{4+} ions. However, in Co–Mn ferrites the spinel structure was maintained after complete reduction beyond 700°C.

The oxidation kinetics in isothermal conditions of Mn^{3+} ions has established that the kinetics is controlled by a diffusion process involving a composition gradient through particles of a nonstoichiometric spinel with a diffusion coefficient depending on the vacancy content. The activation energy of the Mn^{3+} ion oxidation was found to be higher than the activation energy of Fe^{2+} ion oxidation in agreement with their stability toward oxidation (33).

REFERENCES

1. P. Tailhades, P. Mollard, A. Rousset, and M. Gougeon, *I.E.E.E. Trans. Mag.* **26,** 1822 (1990).
2. I. Chassaing, L. Presmanes, P. Tailhades, and A. Rousset, *Solid State Ionics* ***58,*** 261 (1992).
3. E. Kester, B. Gillot, L. Bouet, P. Tailhades, and A. Rousset, *Thermochim. Acta* **261,** 209 (1995).
4. P. Tailhades, Ch. Sarda, P. Mollard, and A. Rousset, *J. Magn. Magn. Mater.* **104–107,** 969 (1992).
5. P. Tailhades, L. Bouet, B. Gillot, P. Mollard, and A. Rousset, "Proceedings of the 6th International Conference on Ferrites, Tokyo," p. 624. 1992.
6. I. Chassaing, L. Presmanes, P. Tailhades, A. Rousset, and P. Mollard, *J. Phys. IV* **2** 127 (1992).
7. B. Gillot and A. Rousset, *Heterogen. Chem. Rev.* **1,** 69 (1994).
8. B. Gillot, M. El Guendouzi, P. Tailhades, and A. Rousset, *React. Solids* **1,** 139 (1986).
9. P. Tailhades, R. Bendaoud, A. R. Fert, A. Rousset, and B. Gillot, *Mater. Chem. Phys.* **17,** 521 (1987).
10. E. M. Vogel, D. W. Johnson, Jr., and P. K. Gallagher, *J. Am. Ceram. Soc.* **60,** 31 (1977).
11. J. M. Jimenez Mateos, J. Morales, and J. L. Tirado, *J. Solid State Chem.* **82,** 87 (1989).
12. B. Gillot, M. El Guendouzi, M. Kharroubi, P. Tailhades, R. Metz, and A. Rousset, *Mater. Chem. Phys.* **24,** 199 (1989).
13. B. Gillot, *J. Phys. Chem. Phys.* **37,** 857 (1976).
14. W. B. White and B. A. DeAngelis, *Spectrochim. Acta, A* **23,** 985 (1967).
15. O. S. Josyulu and J. Sobhanadri, *Phys. Stat. Sol.* (*a*) **65,** 479 (1981).
16. P. Tarte, *Spectrochim. Acta* **19,** 49 (1963).
17. V. A. Potakova, N. D. Zverev, and V. P. Romanov, *Phys. Stat. Sol.* (*a*) **12,** 623 (1972).
18. D. K. Kulkarni, *Curr. Sci. Lett.* **43,** 374 (1974).
19. J. D. Dunitz and L. E. Orgel, *J. Phys. Chem. Solids* **3,** 318 (1972).
20. A. C. C. Tseung and J. R. Goldstein, *J. Mater. Sci.* **7,** 1383 (1972).
21. P. Poix, *Bull. Soc. Chim. Fr.* **5,** 1085 (1965).
22. P. Poix, *C.R. Acad. Sci., Paris* **268,** 1139 (1969).
23. A. Navrostky and O. J. Kleppa, *J. Inorg. Nucl. Chem.* **29,** 2701 (1967).
24. J. L. Baudour, Private communication.
25. B. Gillot, M. Kharroubi, R. Metz, and R. Legros, *Silicates Industriels. Ceram. Sci. Technol.* **59,** 39 (1994).
26. P. Petit, J. Dürr, M. Lenglet, and B. Hannoyer, *Mater. Res. Bull.* **28,** 959 (1993).
27. B. Domenichini, B. Gillot, L. Bouet, and P. Tailhades, *J. Solid State Chem.* **103,** 16 (1993).
28. B. Gillot, D. Delafosse, and P. Barret, *Mater. Res. Bull.* **8,** 143 (1973).
29. M. Nohair, P. Perriat, B. Domenichini, and B. Gillot, *Thermochim. Acta* **244,** 223 (1994).
30. P. Perriat, D. Domenichini, and B. Gillot, *J. Phys. Chem. Solids,* to be published.
31. B. Gillot, A. Rousset, and G. Dupre, *J. Solid State Chem.* **25,** 263 (1978).
32. J. W. D. Martens, *J. Appl. Phys.* **59,** 3820 (1986).
33. B. Gillot, *J. Solid State Chem.* **113,** 163 (1994).